Microchemical Journal 182 (2022) 107878

Contents lists available at ScienceDirect

Microchemical Journal

journal homepage: www.elsevier.com/locate/microc

Electroinduced crosslinking of triphenylamine-based polybenzoxazines

Carolina Gascó, Luis Rodríguez-Santiago, Mariona Sodupe, Rosa María Sebastián *, Gonzalo Guirado *

Departament de Química, Universitat Autònoma de Barcelona, 08193- Bellaterra, Barcelona, Spain

ARTICLE INFO

Keywords:
Polybenzoxazines
Electrochemistry
Electroinduced crosslinking

ABSTRACT

Polybenzoxazines attract much attention as good phenolic resins due to their interesting and useful properties. Recently, benzoxazine monomers have been employed as crosslinking agents to enhance the properties of different types of polymers by being used as additives to a secondary cure process. In this paper, we propose a new electroinduced approach to increase the crosslinking density of electroactive polybenzoxazines through the design of new monomers that contain triphenylamine groups as electrodimerization points. The use of electrochemical techniques means the crosslinking process can be monitored and also the electrochemical reaction process upon polybenzoxazine oxidation either in solution or ionogel matrixes can be disclosed. These studies lay the foundations for the design of smart polybenzoxazines that could undergo dual-cure mechanisms at low electrochemical potential values.

1. Introduction

Crosslinked polymers have been widely investigated due to their interesting thermal and mechanical properties [1]. However, the highly crosslinked matrix that is generated limits post-processing actions, such as annealing, melting [2] and, consequently, potential molding [3], thus hindering some applications. To overcome this problem, dual-cure polymerization has been developed over the years, which consists of starting from a well-designed monomer, and combining two polymerization reactions that happen sequentially. Epoxy-acrylate oligomers cured in two steps (photo and thermal activation) have been described to improve its processability and adhesion properties [4]. Another example based on thiol-acrylate networks involves performing an initial pre-polymerization reaction through Michael addition chemistry followed by a secondary photoinduced free radical polymerization of the acrylate moieties. This substrate is used in impression materials and shape memory polymers [5].

In dual-curing methodologies, in a first step, the main polymer chain is built, and the second polymerization event can be activated by photo [6], free-radical [7], thermally [8] or electrochemically [9] induced polymerization. Despite being a clean stimulus, having a localized action and being an on-demand technique, the electrochemically induced process is the least used. In the example described in the literature, the main chain was functionalized with an electroactive molecule able to form covalent (reversible or irreversible) bonds between themselves when an electric stimulus is applied, resulting in a crosslinked matrix [10]. Triphenylamine (**1**, **TPA**) is a well-defined electroactive unit with the ability to generate electro-coupling when a low oxidative potential is applied. This molecule has been linked to, for instance, polystyrene and polythiophene, arising in electro-induced crosslinking [11] (Scheme S1, supporting information) [12].

Polybenzoxazines, a new kind of phenolic resins, have recently been postulated as useful and relevant polymers due to their notable properties, namely excellent static and dynamic mechanical properties, low water absorption and flammability, near-zero shrinkage or volumetric expansion upon curing, high UV and chemical resistance, and considerable molecule-design flexibility [13]. Benzoxazines are classically obtained from a Mannich type reaction from phenols, formaldehyde, and amines. The possibility of selecting the appropriate groups linked to phenols and amines leads to an extraordinary benzoxazine and polybenzoxazine design versatility, generating thermosets that present interesting properties (Scheme S2.1.) [14].

Benzoxazines have also been used in the dual-curing polymerization process. Scheme S2.2. is a simple illustration of the three different strategies found in the literature. The approach described in Scheme S2.2.a consists of a first polymerization process (PP) of a functionalized monomer obtaining a well-known polymeric main chain as polybutadiene [15], polystyrene [16] and polyvinylchloride [17]. This

* Corresponding authors.
E-mail addresses: rosamaria.sebastian@uab.cat (R.M. Sebastián), gonzalo.guirado@uab.cat (G. Guirado).

https://doi.org/10.1016/j.microc.2022.107878
Received 13 May 2022; Received in revised form 10 August 2022; Accepted 11 August 2022
Available online 19 August 2022
0026-265X/© 2022 The Authors. Published by Elsevier B.V. This is an open access article under the CC BY-NC-ND license (http://creativecommons.org/licenses/by-nc-nd/4.0/).

process is followed by a benzoxazine functionalization of the principal polymer that can crosslink the network after a thermal ring opening polymerization (ROP). In another strategy shown in Scheme S2.2.b, the benzoxazine is functionalized beforehand with radical or photo-induced polymerizable vinyl groups [18] or methacryloyl groups [19] forming, again, the main chain with benzoxazine moieties that polymerize in a secondary step. In the last one, Scheme S2.2.c, the process starts, as before, with a functionalized benzoxazine, but in this case, the first polymerization step is the ROP of benzoxazine, and the second evolves the coupling between the reactive groups, which are linked using, for instance, photo-induced coumarin-coumarin dimerization [20]. The extension of the applicability and the better mechanical properties, durability and stability of the final polymer justified the search for crosslinkable polybenzoxazine matrixes that are already used in anti-corrosion coatings [21] or electronic devices [22]. The crosslinking methodologies of the polymeric part that is not related with the benzoxazine (ROP) are mainly driven by light induced polymerization [23]. Although electrochemical stimulus shares some advantage with the light-induced one, there is a lack of literature related to enhancement of the crosslinking density of polybenzoxazine derivatives using electric stimuli due to the low conductivity of this kind of polymer.

In the current manuscript, we propose the design of electroactive benzoxazine polymers by introducing triphenylamine to their chemical structure, which can undergo σ-dimers through a C—C bond formation upon oxidation [12,24,25] to achieve a crosslinked matrix through an electric stimulus (Scheme S2.2.c). Various possibilities, from triphenylamine derivates to electroactive polybenzoxazine oligomers, have been investigated to control and trigger at low oxidation potential values the crosslinking process of the functionalized polybenzoxazines in solution and in conductive ionogel matrixes.

2. Experimental section

2.1. Materials and methods

Nuclear magnetic resonance (NMR) spectra were recorded using Bruker spectrometers DPX-250, DXP-360 and AVANCE-III 400 (Servei de Ressonància Magnètica Nuclear, UAB): 250 MHz (^{1}H), 62.5 MHz (^{13}C); 360 MHz (^{1}H), 90 MHz (^{13}C); 400 MHz (^{1}H), 100 MHz (^{13}C) respectively. ^{1}H and ^{13}C chemical shifts are reported in ppm relative to tetramethylsilane, using residual ^{1}H and ^{13}C resonances from solvent as internal standards. Infrared spectra were recorded using a Bruker Tensor 27 instrument equipped with an ATR Golden Gate cell and a diamond window. Gel permeation chromatography (GPC) analysis was performed using Agilent Technologies 1260 Infinity hardware using THF as solvent at 1 mL/min. The GPC instrument was equipped with three gel columns: PLgel 5 μm Guard /50 × 7.5 mm), PLgel 5 μm 10000 Å MW 4 K-400 K and PL Mixed gel C 5 μm MW 200–3 M. Oligomeric synthetized polybenzoxazine standards were used to calibrate the GPC (similar results were obtained with commercial polystyrene standards). Bruker MicroFLEX or Bruker AutoFLEX III TOF/TOF as MALDI Mass spectra, Dithranol (DIT) as matrix, and high-resolution mass spectra, using a direct inlet system (ESI). Differential scanning calorimetry (DSC) samples were analyzed with a TA Instrument Q20 using Tzero™ pans and lids calibrated with indium (Tm = 429.75 K, ΔHm = 3267 kJ/mol), scanning rate: 15 °C/min. Thermal gravimetric analysis (TGA) samples were recorded with a Perkin Elmer TGA 8000™.

2.1.1. Synthesis of benzoxazine monomers

6-methoxy-3-methyl-3,4-dihydro-2*H*-benzo[e][1,3]oxazine (B1): Benzoxazine monomer **B1** was synthesized following the procedure described in the literature [26].

3-methyl-*N*,*N*-diphenyl-3,4-dihydro-2*H*-benzo[e][1,3]oxazin-6-amine (B2): To a round flask containing 4 mL of dioxane, formalin (37 % H_2O, 10 % MeOH) (0.40 mL, 4.60 mmol) and methylamine (33 % EtOH) (0.30 mL, 2.30 mmol) were added with continuous stirring in an ice bath for 10 min, after which a solution of 4-(diphenylamino)phenol, **2**, (0.60 g, 2.30 mmol) dissolved in 5 mL of dioxane was added dropwise and the mixture was refluxed (the reaction was followed by ^{1}H NMR). Then, after 24 h, the reaction crude was cooled and 30 mL of diethyl ether was added, and the resulting solution was washed three times with 30 mL of H_2O. The resulting organic phase was dried with anhydrous Na_2SO_4 and the solvent evaporated under reduced pressure. The benzoxazine was purified by flash silica gel column chromatography (7:3 hexane: ethyl acetate v/v) obtaining the desired benzoxazine as a yellow viscous liquid 0.41 g, 56 % yield). ^{1}H NMR ($CDCl_3$, 360 MHz) δ (ppm): 7.25–7.21 (apparent t, J = 7.2 Hz, 4H), 7.06–7.04 (apparent d, J = 7.1 Hz, 4H), 6.98–6.92 (apparent t, J = 7.0 Hz, apparent s, 3H), 6.78–6.74 (apparent m, 2H), 4.79 (s, 2H), 3.87 (s, 2H), 2.63 (s, 3H). ^{13}C NMR ($CDCl_3$, 90 MHz) δ (ppm): 150.8, 148.2, 140.6, 129.1, 125.7, 125.0, 122.9, 121.9, 120.7, 117.2, 83.9, 52.2, 40.0. IR (ATR, cm^{-1}): 3034, 2943, 1585, 1485, 1448, 1427, 1286, 1273, 1228, 1211, 1191, 1143, 1110, 926, 748, 694, 631. HR-ESI-MS (*m/z*): calculated for $C_{21}H_{21}N_2O$, 317.1648; found [M$^+$]: 317.1648.

***N*-(4-methoxyphenyl)-3-methyl-*N*-phenyl-3,4-dihydro-2*H*-benzo[e][1,3]oxazin-6-amine (B3)**: The synthetic procedure and purification of this benzoxazine is similar to **B2**, reaction among **3**, $MeNH_2$ and CH_2O, obtaining 0.53 g of a orange viscous liquid with an 80 % yield. ^{1}H NMR ($CDCl_3$, 360 MHz): 7.19–7.15 (t, J = 7.2 Hz, 2H), 7.06–7.03 (br d, J = 7.0 Hz 2H), 6.95–6.92 (d, J = 6.9 Hz, 2H), 6.90–6.81 (apparent m, 4H), 6.72–6.70 (br d, J = 6.7 Hz, 2H), 4.77 (s, 2H), 3.85 (s, 2H), 3.80 (s, 3H), 2.61 (s, 3H). ^{13}C NMR ($CDCl_3$, 90 MHz): 155.8, 149.8, 148.9, 141.2, 141.1, 129.1, 126.6, 124.9, 124.1, 121.2, 120.7, 120.64, 117.2, 114.8, 83.9, 55.6, 52.3, 40.0. IR (ATR, cm^{-1}): 2944, 2897, 2834, 1486, 1236, 1210, 1032, 924, 821, 749, 695. HR-ESI-MS (*m/z*): Calculated for $C_{22}H_{23}N_2O_2$, 347.1754; found [M$^+$], 347.1750.

Synthesis of compounds 2 and 3.

4-(diphenylamino)phenol (2): Compound **2** was synthesized following procedures similar to those as reported [27].

4-((4-methoxyphenyl)(phenyl)amino)phenol (3):[27] In a 25 mL schlenk, 4-bromophenol (1.20 g, 6.94 mmol), 4-methoxy-*N*-phenylaniline (1.22 g, 6.12 mmol) and sodium *tert*-butoxide (1.60 g, 16.23 mmol) were dissolved in 20 mL of anhydrous toluene. At the same time, in another schlenk, palladium acetate (0.007 g, 0.029 mmol) was dissolved in 20 mL of anhydride toluene. Once it had turned into a solution, tri-*tert*-butylphosphine (0.8 mL, 0.062 g, 0.31 mmol) was added over it. After 5 min, both solutions were mixed using a cannula and the resulting mixture was refluxed for 5 h (the reaction was followed by ^{1}H NMR). After this time, the reaction crude was cooled, toluene was evaporated and, then ethyl acetate (30 mL) was added. The mixture was washed with deionized water (3 × 30 mL), the organic phase was dried over anhydrous Na_2SO_4, and ethyl acetate was removed under reduced pressure. The pure product was achieved by flash column chromatography (silica gel, hexane: ethyl acetate = 7:3 v/v) as a dark blue sticky solid (caramel aspect) (1.70 g, 96 % yield). ^{1}H NMR (acetone-d_6, 360 MHz) δ (ppm): 8.30 (s, 1H), 7.15 (dd, J = 7.1 Hz, 2H), 7.01 (d, J = 7.0 Hz, 2H), 6.95 (d, J = 6.9 Hz 2H), 6.88 (d, J = 6.9 Hz, 2H) 6.84–6.80 (m, 5H), 3.77 (s, 3H). ^{13}C NMR (acetone-d_6, 100 MHz) δ (ppm): 156.7, 154.7, 149.9, 141.9, 140.6, 129.6, 127.9, 127.1, 120.8, 120.8, 116.9, 115.4, 55.6. IR (ATR, cm^{-1}): 3356 (O—H), 3036, 2835, 1593, 1500, 1489, 1460, 1441, 1232, 1178, 1108, 1029, 825, 750, 664. HR-ESI-MS (*m/z*): calculated for $C_{19}H_{17}NO_2$, 291.1254; found [M$^+$]: 291.1251.

Synthesis of compounds 4 and 5.

Both compounds **4** and **5** were synthetized following the same method, whereby the derivative 4-(diphenylamino)phenol (**2** for **4** and **3** for **5**) and benzoxazine **B1** were mixed and heated at 80 °C under continuous stirring forming a black viscous crude. After 24 h, the mixture was cooled and purified by flash silica gel column chromatography (hexane: ethyl acetate 7:3 v/v) obtaining a pale orange solid product (yield = **4**: 53 %; **5**: 38 %).

4: Melting point: 114–120 °C. ^{1}H NMR ($CDCl_3$, 400 MHz) δ (ppm): 7.20 (t, J = 7.1 Hz, 4H), 7.03 (d, J = 8.4 Hz, 4H), 6.97–6.91 (m, 3H),

6.82 (s, 4H), 6.77 (d, $J = 8.4$ Hz, 1H), 3.88 (s, 3H), 3.68 (m, 4H), 2.26 (s, 3H). ^{13}C NMR ($CDCl_3$, 100 MHz) δ (ppm): 154.6, 148.2, 146.6, 144.7, 138.9, 128.9, 126.9, 123.3, 123.2, 122.7, 122.49, 122.45, 121.4, 119.3, 116.8, 110.1, 60.1, 56.1, 55.9, 41.0. IR (ATR, cm^{-1}): 3278 (O—H), 2948, 2833, 1592, 1490, 1239, 1034, 821, 748, 695. HR-ESI-MS (*m/z*): calculated for $C_{28}H_{29}N_2O_3$, 441.2173; found [M^+], 441.2159.

5: Melting point: 140–143 °C. ^{1}H NMR ($CDCl_3$, 360 MHz) δ (ppm): 7.15 (t, $J = 7.17$, 2H), 7.02 (d, $J = 7.03$, 2H), 6.92 – 6.70 (m, 10*H*), 6.64 (br. s, 1H), 3.79 (s, 3H), 3.74 (s, 3H), 3.66 (s, 2H), 3.62 (s, 2H), 2.25 (s, 3H). ^{13}C NMR ($CDCl_3$, 90 MHz) δ (ppm): 155.7, 152.9, 152.7, 150.1, 148.9, 141.3, 140.0, 129.0, 127.5, 126.4, 126.45, 123.5, 120.9, 120.5, 116.6, 116.1, 114.7, 113.9, 59.2, 55.9, 55.6, 41.1. IR (ATR, cm^{-1}): 3254 (O—H), 2949, 2833, 2359, 1592, 1490, 1460, 1432, 1239, 1149, 1107, 1034, 822, 748, 694. HR-ESI-MS (*m/z*): calculated for $C_{29}H_{31}N_2O_4$, 471.2278; found [M^+], 471.2287.

Preparation of polymers 6 and 7

Both polymers were obtained by heating (50–100 mg) of **B2** or **B3** in an open vial at 200 °C for 2 h in a sand bath.

2.1.2. Cyclic voltammetry experiments.

The cyclic voltammetry set-up consisted of a three-electrode system. The working electrode (WE) was a glassy carbon disk of a diameter of 1.02 mm and the counter electrode (CE) was a glassy carbon disk (d = 3 mm). All the potentials were recorded using a CHI600E, *vs* saturated calomel electrode (SCE), isolated from the WE by a salt bridge. Tetrabutylammonium hexafluorophosphate ($TBAPF_6$) 0.1 M was used as the supporting electrolyte at room temperature.

Solutions were prepared using acetonitrile and a mixture of acetonitrile and toluene 1:1 in anhydrous conditions obtained using molecular sieves 3 Å as a drying agent (24 h in activated molecular sieves).

2.1.3. Controlled-potential electrolysis

The set-up for electrosynthesis is a three-electrode system including a carbon graphite rod as WE, a platinum rod as CE separated from the solution by a salt bridge ended with a frit and a saturated calomel electrode as a reference. Electrolysis experiments at controlled potentials were undertaken with an EG&G Princeton Applied Research (PAR) 273A potentiostat and a conical electrochemical cell equipped with an argon bubbling source. All these electrochemical measurements were performed in dry acetonitrile solution containing 0.1 M of $TBAPF_6$ as a supporting electrolyte and at room temperature. Crude obtained after electrosynthesis was directly analyzed by high resolution liquid chromatography-mass spectrometry (LC-MS). The chemicals obtained during electrolysis were isolated by flash silica gel column chromatography and characterized.

Synthesis and characterization of dimers obtained by controlled-potential electrolysis

Compound 9:

To 25 mM of **2** in anhydrous acetonitrile in $TBAPF_6$ 0.1 M under continuous flow of N_2, was applied a controlled-potential of 0.94 V *vs* SCE until 1F (enough charge to oxidise completely **2**). The electrolysis mixture was evaporated, and the residue was flash chromatografied in gel of silica using toluene as eluent. Product **9** was isolated in 26 % yield. Melting point: 100–120C. ^{1}H NMR (acetone-d_6, 400 MHz) δ (ppm): 8.33 (s, 2H), 7.50 (d, $J = 8.7$ Hz, 4H), 7.25 (t, $J = 7.8$ Hz, 4H), 7.02 (m, 12H), 6.96 (t, $J = 7.4$ Hz, 2H), 6.86 (d, $J = 8.7$ Hz, 4H). ^{13}C NMR (acetone-d_6, 100 MHz) δ (ppm): 154.6, 148.2, 147.2, 139.3, 133.6, 129.1, 127.9, 126.9, 122.6, 122.3, 121.8, 116.3. IR (ATR, cm^{-1}): 3316 (O—H), 3029, 2919, 1590, 1486, 1222, 819, 721, 693. HR-ESI-MS (*m/z*): calculated for $C_{36}H_{28}N_2O_2$, 520.2145; found [M^+], 520.2119.

Compound 10:

To 25 mM de OMeTPAOH in anhydrous acetronitrile in $TBAPF_6$ 0.1 M under continuous flow of N_2, was applied a controlled-potential of 0.83 V *vs* SCE until 1F (enough charge to oxidise completely **3**). The electrolysis mixture was evaporated, and the residue was flash chromatografied in gel of silica using toluene as eluent. Product **10** was isolated in 15 % yield. Melting point: 100 – 120 °C. ^{1}H NMR (acetona-d_6, 400 MHz) δ (ppm): 8.25 (s, 2H), 7.42 (d, $J = 8.7$ Hz, 4H), 7.05 (d, $J = 8.6$ Hz, 4H), 6.98 (d, $J = 8.8$ Hz, 4H), 6.90 (d, $J = 8.7$ Hz, 4H), 6.88 (d, $J = 8.6$ Hz, 4H), 6.82 (d, $J = 8.8$ Hz, 4H), 3.78 (s, 6H). ^{13}C NMR (acetone-d_6, 100 MHz) δ (ppm): 156.9, 154.9, 148.7, 141.8, 140.6, 133.2, 128.0, 127.4, 127.2, 121.0, 117.0, 115.5, 55.7. IR (ATR, cm^{-1}): 3315 (O—H), 2921, 2852, 1603, 1490, 1460, 1314, 1235, 1177, 1031, 818. HR-ESI-MS (*m/z*): calculated for $C_{38}H_{32}N_2O_4$, 580.2357; found [M^+], 580.2336.

2.1.4. Spectro-electrochemical experiments

In a range of 3–5 mM solutions of a mixture of acetonitrile and toluene with $TBAPF_6$ 0.1 M were analyzed in a 0.33 mm thin-layered quartz glass cell using platinum gauze and platinum wire as working and counter electrodes, respectively. A saturated calomel electrode (SCE) was employed as a reference electrode. A PC-controlled VSP-Potentiostat synchronized with a monolithic miniature spectrometer (MMS) UV − vis high speed diode array spectrometer with a bandwidth of 300–1100 nm and a deuterium/ tungsten light source coupled to an optical fiber was employed to register the spectroelectrochemical measurements. BioKine32 software was used for data acquisition and treatment.

2.1.5. Computational methods

Quantum mechanical calculations were performed using the B3LYP-D3 method, that is, the B3LYP functional [28–30] plus Grimme's correction (D3) for dispersion forces [31] and the 6-31G(d,p) basis set with the Gaussian 16 package [32]. Solvent effects (toluene) were taken into account using the SMD [33] implicit solvation model.

NPT molecular dynamics (MD) simulations at 300 K were performed with the Amber 16 package [34] using the GAFF force field [35]. Point charges for the solute (polybenzoxazines) and solvent (toluene) molecules were obtained through RESP [36,37] calculations at the optimized B3LYP-D3/6-31G(d,p) minima in implicit toluene using Gaussian 16. The B3LYP-D3/6-31G(d,p) structures optimized in toluene were also used as starting points for the MD simulations. The solute molecules were solvated in a cubic box of size L = 50 Å (L = 60 Å in the case of the hexamers), which was treated under periodic boundary conditions while ensuring that the model reproduced the density of toluene at ambient conditions. The size of the box guarantees a minimum of 24 Å buffer between two solvent molecules. The following equilibration scheme was used: (i) initial minimization in two steps. 5000 points with the steepest descent method fixing the solute and then 5000 more points, 2500 with steepest descent and 2500 with conjugated gradient, relaxing the whole system; (ii) 200 ps of NVT dynamics raising the temperature from 0 to 300 K keeping the solute fixed with weak restraints (force constant of 500 kcal mol^{-1} $Å^{-2}$ on all atoms of the solute); (iii) 2 ns of NPT dynamics at 300 K with no constraints; (iv) 400 ns of NPT production time simulation at 300 K with a time step of 1 fs, the Andersen temperature coupling scheme [38] and the Berendsen barostat [39].

To analyze the results, 2000 equally spaced frames along the simulations were extracted. Based on the RMSD values, the 2000 structures were grouped into conformationally related families using the ensemble cluster scheme [40] implemented in the Chimera package [41] Only the carbon and nitrogen atoms of the polybenzoxazine moiety were considered for the calculation of the RMSD. Finally, the method also identified the most representative structure of each family or cluster.

3. Results and discussion

In this work we will disclose the electroinduced crosslinking mechanism of redox polybenzoxazines, which contain triphenylamine moieties in their skeleton. However, prior to analyze these complex systems, model molecules are previously studied being most of them prepared and investigated for the first time.

3.1. Synthesis of triphenylamine derivatives

In this work we were interested in studing polybenzoxazines containing in their structures triphenylamine moieties. However, to analyse these complex systems, model molecules were previously studied, and some of them were prepared for the first time. Triphenylamine, **1** (**TPA**), was commercially available, whereas -compounds **2** and **3** were synthetized following a Pd-catalyzed *N*-arylation reaction (Scheme 1a). Compounds **4** and **5**, model molecules of polybenzoxazine structures, were obtained by heating in bulk using the described triphenylamines (**2**, **3**) [27] and 6-methoxy-3-methyl-3,4-dihydro-2*H*-benzo[e][1,3] oxazine (**B1**) as synthetized previously in our group [26]. Here, an intrinsic ring opening of oxazine favors the attack of the *orto*-activated phenolic ring, obtaining both compounds (Scheme 1a). Column chromatography purifications were carried out to eliminate side polymerization reactions of the starting reagents. New compounds were characterized as indicated in the experimental section.

Scheme 1b describes the synthesis of polybenzoxazines from triphenylamine monomeric benzoxazines. First, compounds **2** and **3** reacted with methylamine and formaldehyde through a Mannich type reaction [42] yielding benzoxazines **B2** and **B3**. Later, these two benzoxazines were heated in bulk, and after a ring-opening polymerization (ROP) process polybenzoxazines **6** and **7** were obtained without any loss of weight after 2 h at 200 °C. Similar *N*-Ph **B2** benzoxazine have been synthesized from aniline and thermal polymerized to be studied as electrochromic material [43].

Finally, polymeric mixtures were identified and characterized using proton nuclear magnetic resonance (^{1}H NMR). The characteristic signals related with the methylenes belonging to the oxazine ring of monomer disappear when polymerization occurs, so it is easy to follow the ROP mechanism through NMR experiments. Fourier Transform Infrared Spectroscopy (FT-IR) is a great tool to determine the benzoxazine formation, its structure and the polymerization process [44,45]. Peaks assigned to benzoxazine at 1230 cm^{-1} (C—O—C antisymmetric stretching mode of the oxazine ring) and 910–940 cm^{-1} (benzene ring mode with oxazine ring) clearly decreased during polymerization process, indicating the ring-opening reaction of oxazine ring occurred. New bands appeared in the interval of 3300–3500 cm^{-1} corresponding to new generated hydrogen-bonded hydroxyls of open oxazine ring species. An increase in the aliphatic CH at 2927 cm^{-1} that joined the phenolic derivatives to each other was also observed. Thermogravimetry analysis (TGA) and differential scanning calorimetry (DSC) enable determination of the behavior of the intrinsic compounds against a heat flow. Gel permeation chromatography (GPC) was used to determine the distribution of weight corresponding to each polybenzoxazine. For both oligomers, **6** and **7**, three major distributions were obtained in tetrahydrofuran (see supporting information). The deconvolution of the GPC distribution for the synthesis of **6** revealed a c.a. 1 % of opened monomer derivative (**6a**), 29 % of trimer (**6b**) and 70 % of oligomer of five units (**6c**); whereas GPC distribution for **7** showed 8 % of opened monomer (**7a**), 39 % of trimer (**7b**) and 53 % of oligomer of five units (**7c**) in oligomer mixtures, respectively (Scheme 1c).

3.2. Electrochemical behavior of triphenylamine derivatives

Fig. 1a shows a typical cyclic voltammogram of commercial triphenylamine (**1**), using an acetonitrile: toluene solution containing 0.1 M of supporting electrolyte ($TBAPF_6$) in an inert atmosphere. A one-electron wave was observed on the first anodic scan at 1.06 V *vs* SCE, whereas two reduction waves at 0.90 V and 0.73 V *vs* SCE were detected in the corresponding cathodic counter scan. In a second scan (Fig. 1a, dotted line), it was possible to establish the reversibility of at least this second reduction peak (0.73 V *vs* SCE). According to results published previously in similar solvents [12,25], the new peak that appeared in the second cycle after the first oxidation of **1** corresponds to dimerization of triphenylamine radical cation ($\mathbf{1}^{\cdot+}$) leading to *N*, *N*, *N*', *N*'-tetraphenylbenzidine (**8**). To confirm these results, compound **8** was prepared following a previously described synthetic procedure [46]. A cyclic voltammogram of a pure sample of **8** under the same previously described experimental conditions confirmed the formation of **8** after the oxidation of **1** (Fig. 1b). The electrochemical oxidation mechanism of **1** in an acetonitrile: toluene media was fully elucidated by spectroelectrochemical measurements.

Spectroelectrochemical experiments were performed to record the UV–visible absorption spectrum profile of the electrochemically generated transient intermediates. A platinum gauze electrode is utilized to transmit a light beam as an OTE working electrode in a 0.05 cm thick quartz cell. The UV–visible spectra were recorded while a controlled-potential electrolysis at 1.03 V *vs* SCE was occurring for 100 s (Fig. 1c). It can clearly be seen that new absorption bands at 650 and 482 nm developed in the spectrum. In accordance with previous studies [12] these bands can be attributed to $\mathbf{1}^{\cdot+}$ and $\mathbf{8}^{2+}$, respectively. Fig. 1d shows the spectroelectrochemical response of a pure **8** sample, whereby the reversible appearance of the absorption band at 482 nm upon oxidation (1.03 V *vs* SCE – 150 s) and reduction (0.00 V *vs* SCE – 200 s) confirmed the presence of $\mathbf{8}^{2+}$ in the electrochemical oxidation mechanism of **1**.

Once the electrochemical behavior of **1** was determined, the electrochemical behaviour of electroactive units **2** and **3** was fully disclosed using cyclic voltammetry, controlled potential electrolysis and spectroelectrochemistry. Fig. 1e (solid line) shows a reversible oxidation wave, the anodic peak potential value being located at 0.81 V *vs* SCE. In the corresponding counter cathodic scan, a reversible reduction peak could be detected at 0.73 V. This cathodic peak was assigned to the reduction of $\mathbf{2}^{\cdot+}$ which could generate a dimer compound, as was previously observed for the electrochemical oxidation process of **1**. To verify that hypothesis, a controlled potential electrolysis of **2** at 0.94 V was performed, after the passage of 1F dimer **9** was isolated from the reaction crude in a 26 % yield (Scheme S3). The redox behavior of a pure sample of **9** is depicted in Fig. 1e (dotted line) where two successive oxidation reversible waves were measured at 0.74 and 0.86 V *vs* SCE. Finally, when spectroelectrochemical experiments were performed, a new absorption band appeared at 578 nm after applying a 1.00 V constant potential for 100 s. In this case, the only intermediate detected at this time scale was $\mathbf{2}^{\cdot+}$ (Fig. 1f) related to the maximum at 578 nm. Hence, the presence of a hydroxy group, and an electrodonating group by resonance, not only diminishes the oxidation potential value of the triphenylamine but also stabilizes the radical cation formed upon oxidation.

In this regard, in 4-((4-methoxyphenyl)(phenyl)amino)phenol (**3**) the presence of a methoxy group would also increase the stability of its radical cation ($\mathbf{3}^{\cdot+}$) as well as reducing its oxidation potential value. Cyclic voltammetry experiments confirmed that the compound showed a single one-electron reversible wave at 0.71 V *vs* SCE (Fig. 1g, solid line). Note that at this time scale no presence of its corresponding dimer **10** is observed since no reduction peaks were detected in the cathodic counter scan. The formation of $\mathbf{3}^{\cdot+}$ was also confirmed by spectroelectrochemistry, whereby an absorption band appeared at 525 nm when the sample was electrolyzed at 0.90 V *vs* SCE (Fig. 1h). Finally, when long time scale electrochemical experiments were performed, such as controlled potential electrolysis at 0.83 V *vs* SCE, the corresponding dimer **10** was isolated in a 15 % yield (Scheme 2 supporting information). Fig. 2g (dotted line) shows the cyclic voltammogram of a pure sample of **10**, revealing two reversible one electron waves corresponding to the successive formation of $\mathbf{10}^{\cdot+}$ and $\mathbf{10}^{2+}$ at 0.47 and 0.71 V *vs* SCE, respectively.

At this point, it is possible to conclude that compounds **2** and **3** follow the same electrochemical oxidation mechanism as previously disclosed for triphenylamine (**1**), and it was depicted in Scheme S1. The overall process is summarized in Scheme S2 supporting information.

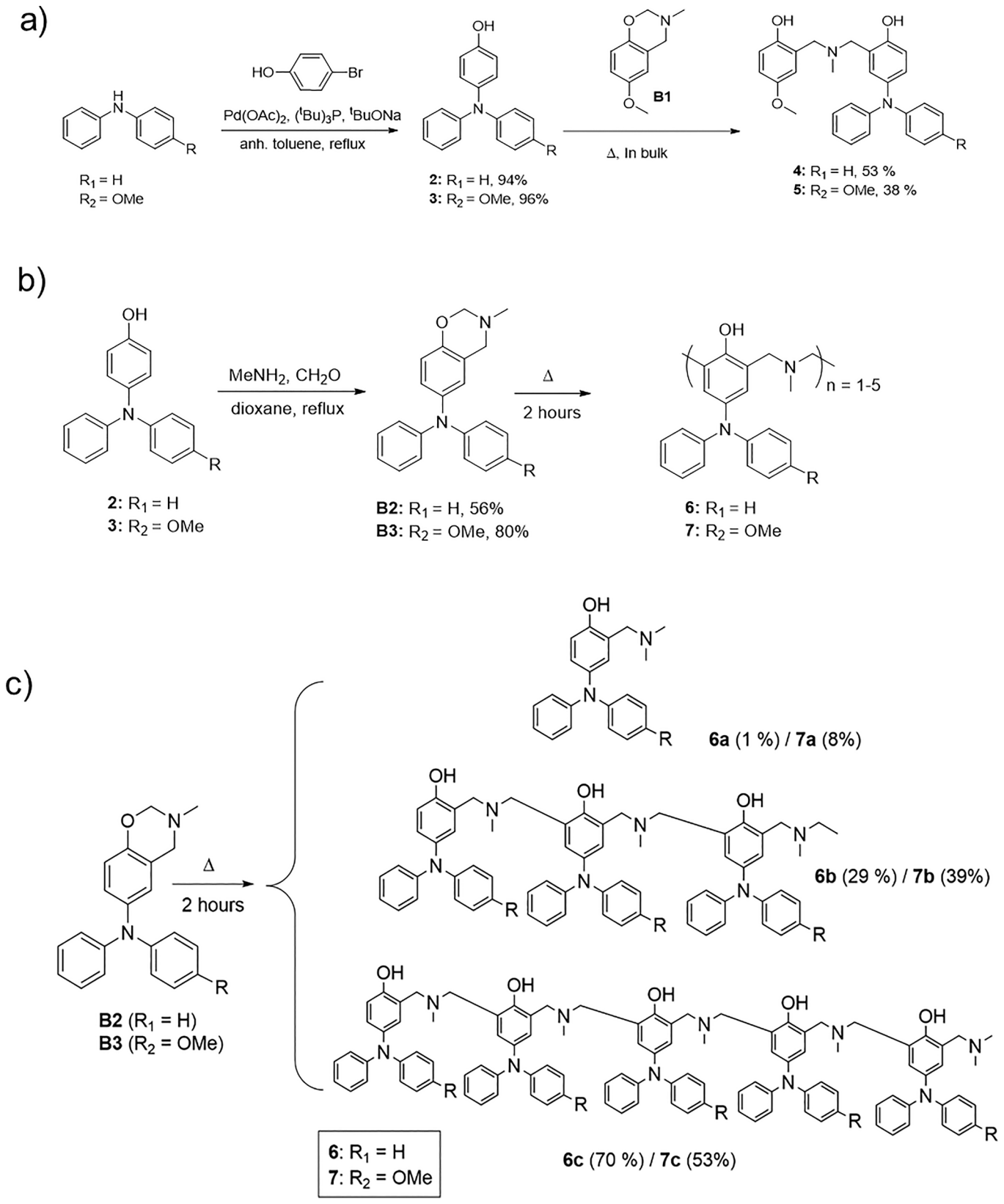

Scheme 1. a) Synthetic route of compounds **2**, **3**, **4** and **5**b) Synthetic route to obtain electroactive benzoxazines, **B2** and **B3**, and polybenzoxazines **6** and **7**c) Oligomer distribution of **6** and **7**.

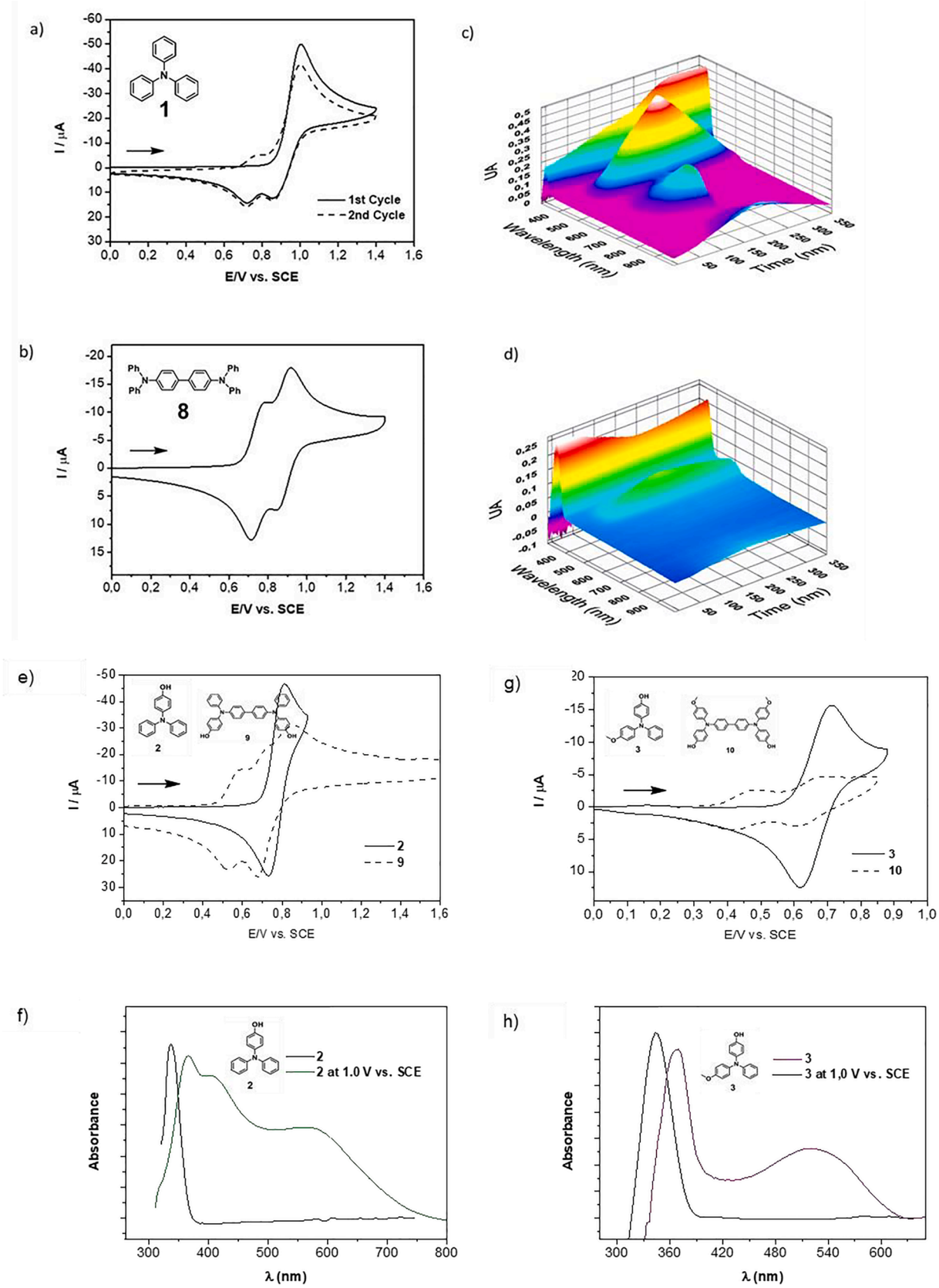

Fig. 1. a) Cyclic voltammograms of 5 mM solution of **1** and (b) 3 mM of **8** acetonitrile:toluene (0.1 M $TBAPF_6$; scan rate = 0.5 V s^{-1}). c) Spectroelectrochemistry of 2 mM **1** and (d) **8** acetonitrile:toluene (0.1 M $TBAPF_6$) (e) Cyclic voltammograms of **2** (6 mM) and **9** (2 mM) in acetonitrile:toluene (0.1 M $TBAPF_6$; scan rate = 0.5 V s^{-1}); (f) UV–vis of initial compound **2** (2 mM) and its spectrum after applying 1.0 V *vs* SCE to acetonitrile:toluene (0.1 M $TBAPF_6$) for 100 s; (g) Cyclic voltammograms of **3** (3 mM) and **10** (2 mM) in acetonitrile:toluene (0.1 M $TBAPF_6$; scan rate = 0.5 V s^{-1}); (h) UV–vis initial compound **3** (2 mM) (t = 0 s) and its spectrum after applying 1.0 V *vs* SCE to acetonitrile:toluene (0.1 M $TBAPF_6$) for 100 s.

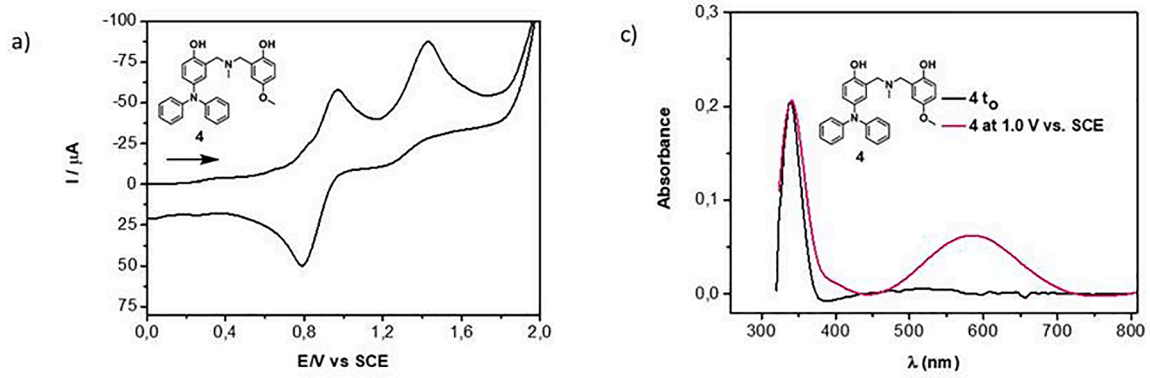

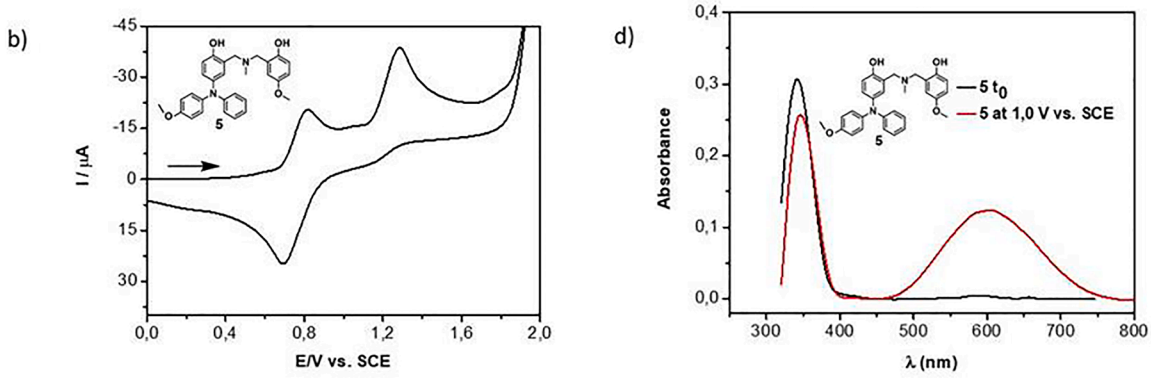

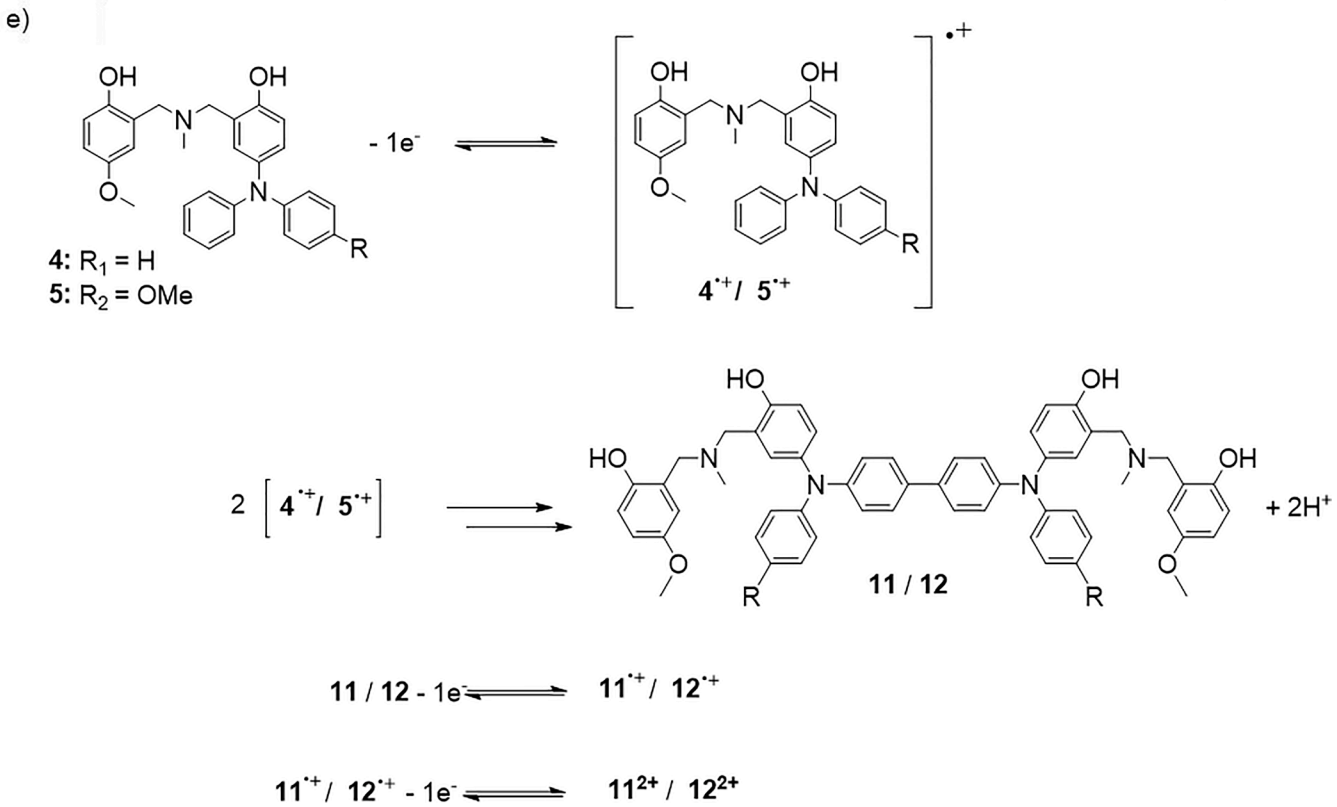

Fig. 2. Cyclic voltammograms of 3 mM (a) **4** and (b) **5** in acetonitrile:toluene (0.1 M $TBAPF_6$; scan rate = 0.5 V s^{-1}). UV–vis spectrum of 2 mM of (c) **4** and (d) **5** at initial state (t_o = 0 s) and after applying 1.0 V in acetonitrile:toluene (0.1 M $TBAPF_6$) (e) Proposed electroinduced coupling for compounds **4** and **5** to generate compound **11** (R_1 = H) and **12** (R_2 = OMe).

3.3. Electrochemical behavior of triphenylamine-polybenzoxazine derivatives

Prior to studying the complex electroactive polybenzoxazines, simple models **4** and **5** (Scheme 1) were analyzed to determine whether the radical cation of those compounds followed a dimerization mechanism. Compounds **4** and **5** showed a very similar redox and optical behavior (Fig. 2). In both cases, in the first anodic scan two oxidation peaks were observed, which led to the formation of their respective cation radical and dication. Note that in both cases the first oxidation peak at 0.97 (Fig. 2a) and 0.80 V (Fig. 2b) corresponds to a pseudoreversible peak, its current function being slightly higher than one electron. Spectroelectrochemistry experiments show an absorption band at 584 (Fig. 2c) and 604 nm (Fig. 2d), which corroborates the existence of the intermediates $\mathbf{4}^{\cdot+}$ and $\mathbf{5}^{\cdot+}$, respectively, upon controlled potential oxidation at 1.0 V. However, a closer look at the cathodic scan of cyclic voltammograms (Fig. 2a and 2b) reveals that the current values associated to those cathodic peaks are higher than those previously observed in the first anodic scan. These results can be rationalized considering how the oxidized forms of dimers $\mathbf{11}^{\cdot+}$ and $\mathbf{12}^{\cdot+}$, which are formed during oxidation of **4** and **5**, are reduced at the same potential value as $\mathbf{4}^{\cdot+}$ and $\mathbf{5}^{\cdot+}$. The current function of the cathodic peaks is increased in the reverse scan. In Fig. 2e, the proposed electroinduced dimerization process is shown for compounds **4** and **5**, presenting the redox intermediates described above.

Those results were confirmed by controlled-potential electrolysis (Scheme S4). The analysis of the high-performance liquid chromatography of the reaction crudes coupled with high resolution mass spectrometry confirmed the formation of the corresponding σ-dimers **11** and **12** formed upon oxidation of **4** and **5** after the passage of 1F at 1.20 V and 1.00 V, respectively.

Having demonstrated that two-unit triphenylamine-polybenzoxazine models (**4** and **5**) undergo an electroinduced dimerization process, triphenylamine-polybenzoxazine oligomers **6** and **7** were synthetized from **B2** and **B3**, respectively, in bulk under heating through a ring-opening polymerization (Scheme 1c). The above-mentioned product distributions were well correlated by cyclic voltammetry experiments (Fig. 3a and Fig. 3b). In both cases, three different oxidation peaks at 0.89 V, 0.99 V and 1.14 for **6** and 0.80 V, 0.87 V and 0.94 V for **7** were observed. As expected, the presence of a methoxy electrodonating group in the diphenylamine structure of the polymer makes it easier to oxidize the polybenzoxazine derivative. The total number of electrons involved in this first electron transfer process were 1.67 and 1.87 for mixtures **6** and **7**, respectively. These results seem to indicate that there is a C—C coupling process and an electron transfer at the same potential, as it has been previously noted for two-units of triphenylamine-polybenzoxazine derivatives. Spectroelectrochemistry of polybenzoxazine **6** (Fig. 3c) shows the formation of $\mathbf{6}^{\cdot+}$ at 650 nm as well as an intense band at 458 nm that could be associated with the oxidized dimers $\mathbf{6}^{2+}$. The same results were obtained when control potential spectroelectrochemical experiments were performed after the first oxidation wave for **7**, whereupon the formation of radical cations $\mathbf{7}^{\cdot+}$and dimers $\mathbf{7}^{2+}$ at 604 nm and 465 nm, respectively, were also detected (Fig. 3d). Thus, an electroinduced crosslinking process may occur through the formation of σ-dimers in **6** and **7** polymeric mixtures.

In order to confirm electroinduced crosslinking via a triphenylamine radical cation coupling process, we decided to use compound **6** since it has a larger number of free coupling positions in its structure. Thus, a controlled potential electrolysis of **6** in an acetonitrile: toluene (1:4) (0.1 M of $TBAPF_6$) solution was performed at 1.20 V *vs* SCE. For polymeric mixture **6** after the passage of 3F, the crude of electrosynthesis was evaporated and digested in acetonitrile for 24 h to eliminate $TBAPF_6$, and filtered. The solid obtained was suspended in clean acetonitrile and centrifugated for 3 min at 3000 rpm; this process was repeated three times to remove completely the soluble salt. The remaining solid was dried and characterized by proton nuclear magnetic resonance (^{1}H NMR), differential scanning calorimetry (DSC) and thermogravimetric analysis (TGA). Although no significant changes were observed in ^{1}H NMR spectrum before and after oxidation of **6** (Fig. 3e), DSC and TGA analysis revealed significant changes. The DSC experiments depicted in Fig. 3b revealed an increase in the Tg from the electrolyzed sample (Tg (**6**) = 75.6 °C; Tg (**E6**) = 109.6 and 162.7 °C, Fig. 3f). This phenomenon is attributed to a more crosslinked polybenzoxazine that is supported by TGA experiments (Fig. 3c and Fig. 3h), in which the degradation temperature observed for 5 and 10 % of weight loss was higher in the electrolyzed sample; char yield was also increased in more than 10 % (Fig. 3g,h) [47]. Hence, our experiments indicate that crosslinking of the material through electrodimerization of electroactive moieties incorporated in polybenzoxazine **6** was achieved.

To shed light on the structure of the functionalized polybenzoxazines, we selected trimers **6b** and **7b** as models and performed atomistic molecular dynamics (MD) simulations and DFT calculations. Figure S1 shows the initial quantum mechanics (QM) optimized linear structures for both systems. These structures were used as the starting point for the molecular dynamics simulations. RMSD values along MD simulation are shown in Figure S2. The results of the simulations show that the preferred arrangement for the trimers involves a central core with the phenol and amine groups of the polybenzoxazine moiety interacting through a network of hydrogen bonds and the diphenylamine groups pointing to the solvent. Analysis of the intramolecular H-bonds throughout the trajectory shows that they are labile, and the main interactions include O—H···OH and O—H···N contacts. Values presented in table S1 indicate that the former are more frequent, probably due to entropic factors because OH···N ones imply more folded structures, as shown in previous studies for other polybenzoxazines [48].

Cluster analysis of the trajectories was carried out to obtain representative structures of the systems. Figure S3 shows the population of each cluster for both **6b** and **7b** MD simulations, and Table 1 (first row) shows the representative structure of the most populated cluster for each system, with the network of H-bond highlighted. As commented above, diphenylamine groups are exposed to the solvent and are thus available for crosslinking with neighbor oligomers, thus favoring polymerization. It should also be noted that diphenylamine groups belonging to the same oligomer are far apart, thus preventing intramolecular crosslinking. Representative structures for other clusters with significant populations are also shown in Figures S4 and S5.

To determine the most prone position/s for polymerization through σ-dimerization after oxidation of the sample, oxidized structures of the trimers were also computed. These structures were obtained by oxidizing the corresponding representative structure of the most populated cluster of **6b** and **7b** at the QM level (see Figures S6 and S7) and reoptimizing at the same level of theory. The results show that the geometries do not change significantly after oxidation. The spin density is completely delocalized among the aromatic rings, computed values being around 0.1 a.u. in each of the nine aromatic rings. Within the aromatic ring, the largest value (~0.05 a. u.) corresponds to the phenyl carbon atoms in *para* with respect to the substituted carbon, of external aromatic rings. Therefore, one would expect dimerization to occur through these carbon atoms. Consequently, as a model for the polymer we used a hexamer structure obtained by joining two molecules of **7b** through this carbon atom of the *N*-terminal monomers. The geometry of the resulting hexamer was optimized at the DFT level and used as starting points for the MD simulations as a model case.

Table 1 (second row) shows the representative structure of the most populated cluster. The system behaves as two independent trimers connected by a biphenyl bridge at the *para* position. That is, each trimer subunit is arranged around a central core where the OH and the amino groups interact through hydrogen bonds. However, it should be noted that the hydrogen bonds are more labile than in the previous case, and most of the structures do not show three hydrogen bonds per unit. The terminal aromatic rings that are not involved in the bridge between subunits are exposed to the solvent or, in some cases, aligned with the

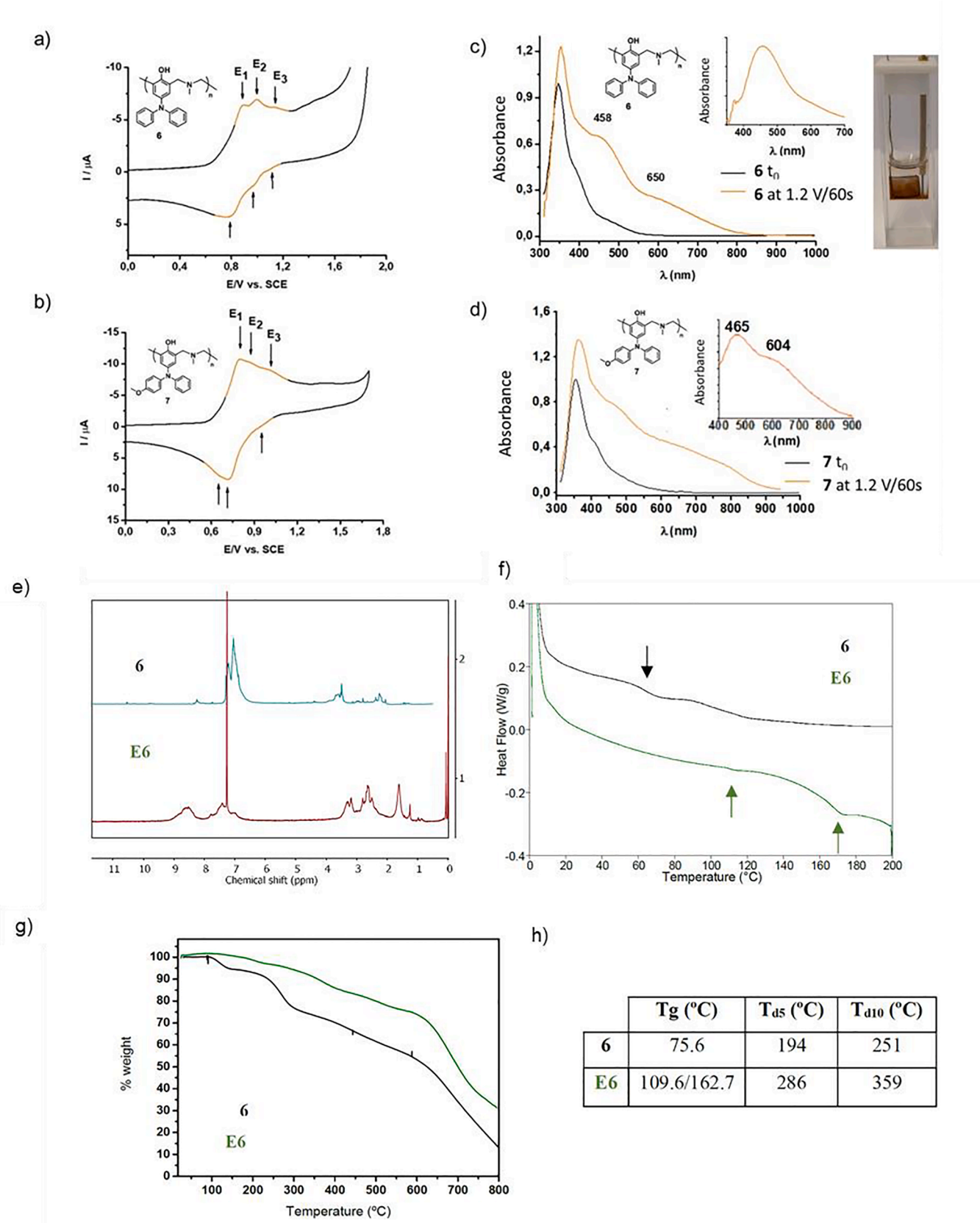

	Tg (°C)	T_{d5} (°C)	T_{d10} (°C)
6	75.6	194	251
E6	109.6/162.7	286	359

Fig. 3. Cyclic voltammograms of 1.3 mM (a) **6** and 2.1 mM of (b) **7** in acetonitrile:toluene (0.1 M $TBAPF_6$; scan rate = 0.5 V s^{-1}). UV–vis spectrum of 10 mM of (c) **6** and (d) 7 at initial state and after applying 1.2 V to acetonitrile:toluene 1:4 (0.1 M $TBAPF_6$) (e) ^{1}H NMR spectrum, (f) DSC thermogram, and (g) TGA thermograms of compound **6** before and after the electrosynthesis process (**E6**) (h) Table with glass transition and degradation temperatures at 5 % and 10 % loss of weight.

Table 1
Representative structure of the most populated cluster of DFT simulations of **6b**, **7b** and representative structure of the most populated cluster of the MD simulations of the hexamer resulting from the crosslink of two **7b** trimer molecules.

Structure 6b	Structure 7b
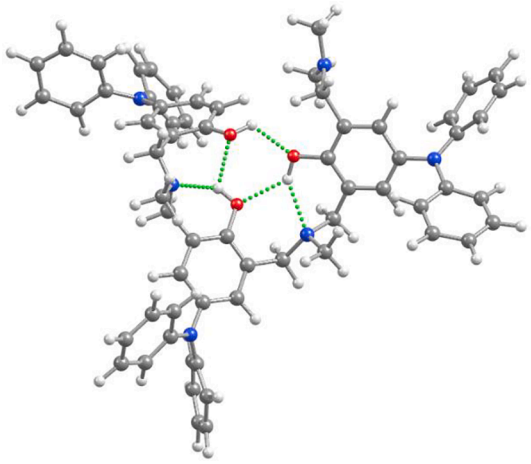	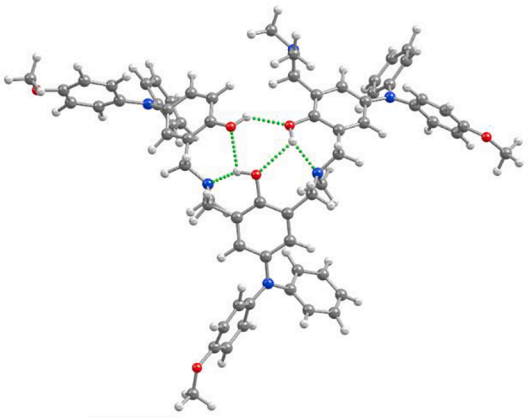

Trimer of Structure **7b**

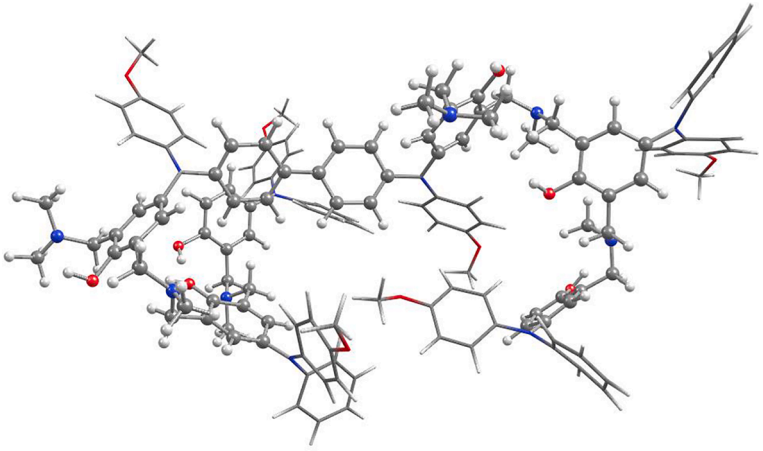

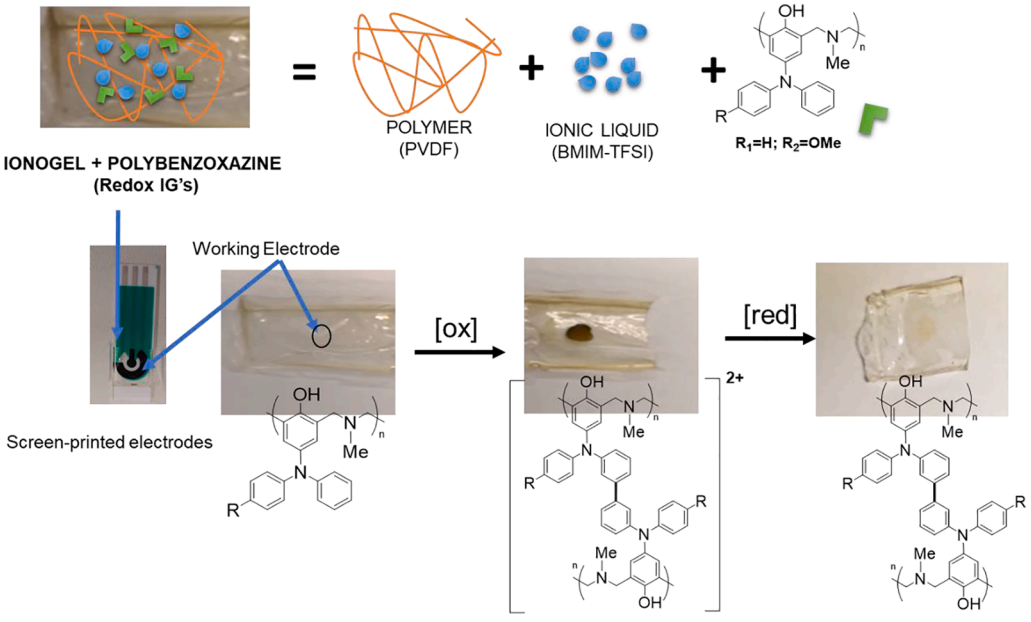

Fig. 4. Redox polybenzoxazine system in polymeric gel electrolytes.

other subunit. In this sense, several structures show small distances between aromatic rings of both subunits (for example in clusters 1 and 2), which is also in good agreement with the possibility of an intramolecular crosslink in a subsequent oxidation.

3.4. Electroinduced crosslinking process of triphenylamine-polybenzoxazine oligomers in ionogel matrixes

As a proof of concept to work in a solid state, we decided to introduce the redox polybenzoxazine systems to polymeric gel electrolytes, ionogels (IGs), based on poly(vinylidenefluoride-*co*-hexafluoropropylene (P(VDF-*co*-HFP)) and ionic liquids (ILs). Those IGs would act as a solid matrix as well as electrolytes introducing flexibility, elasticity, and high ionic conductivity [49] to improve the brittle and isolating polybenzoxazine materials. Based on previous results obtained in our research group [50,51], for this study an IG composed of P(VDF-*co*-HFP) - [BMIM][TFSI] at a weight ratio of 1:5 was selected since it shows enough ionic conductivity, transparency, and flexibility. A mixture of P(VDF-*co*-HFP) - [BMIM][TFSI] and polybenzoxazine at a weight ratio of 1:5:0.5 was solved in acetone and dried at room temperature. Hence, the resulting triphenylamine-polybenzoxazine IGs was stuck onto screen-printed electrodes. These commercially available electrodes consist of a carbon ink for working and counter electrodes and silver/silver chloride screen-printing paste for the reference electrode (Fig. 4). As can be observed, after applying an oxidative redox potential (1.20 V *vs* Ag/AgCl) there is a change in the color of the modified IG located on the surface of the working electrode. This coloration appears because of the oxidation of generated species that can absorb at the visible range of the spectrum. The maximum wavelength obtained in the spectrum for compound **6** can be attributed to the formation of σ-dimers ($\mathbf{6}^{2+}$), as was previously observed in solution. The modified IGs lose their color after reducing (to 0.00 V *vs* Ag/AgCl) the charge σ-coupling intermediates of $\mathbf{6}^{2+}$ to their colorless neutral-state σ-dimers (Fig. 4). The same results were observed when compound **7** was used instead of compound **6**. At this point, it is possible to envisage that either a cut or damage to those redox polybenzoxazine IGs materials can easily be electrochemically crosslinked through a dimerization process. Besides, the fact that triphenylamine-polybenzoxazine materials are electrochromic means there is a change of color on applying a redox potential, thus enabling quick naked-eye analysis and checking of the crosslinking processes.

4. Conclusions

Triphenylamine derivatives undergo an electrochemical oxidation dimerization mechanism at low oxidation potential values. The stability of the corresponding radical cations as well as the dimerization points can be tuned and controlled depending on the number and type of substituents present in the redox center. The design of new redox triphenylamine-polybenzoxazine systems by incorporating triphenylamine moieties in the benzoxazine backbone not only means these polymers can be oxidized at low oxidation potential values but also leads to a dimerization process of their units in solution. Hence, it has been demonstrated that crosslinking of benzoxazine oligomeric units can easily be achieved by applying an electric stimulus either in solution or solid state. DFT calculations reinforce experimental results. These studies lay the foundations for the design of smart polybenzoxazines that are able to undergo crosslinking at low electrochemical potential values using ionogel matrixes.

Declaration of Competing Interest

The authors declare that they have no known competing financial interests or personal relationships that could have appeared to influence the work reported in this paper.

Data availability

Data will be made available on request.

Acknowledgements

The authors are grateful for financial support from projects PID2019-106171RB-I00 and PID2020-112715 GB-I00 of the Ministerio de Ciencia e Innovación (MICINN). C.G. and also to the Spanish Ministry of Science, Innovation and Universities for the award of a research studentship via the FPI program (BES-2016-078179) and to Spain's MEC (CTQ2016-81797-REDC and RED2018-102387-T), the ORFEO CINQA Network and for funding from DURSI-Generalitat de Catalunya (2017- SGR465).

Appendix A. Supplementary data

Supplementary data to this article can be found online at https://doi.org/10.1016/j.microc.2022.107878.

References

[1] D. Kuckling, A. Doering, F. Krahl, K.-F. Arndt, 8.15 - Stimuli-Responsive Polymer Systems, Editor(s): Krzysztof Matyjaszewski, Martin Möller, Polymer Science: A Comprehensive Reference, Elsevier (2012) 377–413, https://doi.org/10.1016/B978-0-444-53349-4.00214-4.

[2] A.R. Kannurpatti, K.J. Anderson, J.W. Anseth, C.N. Bowman, Use of "living" radical polymerizations to study the structural evolution and properties of highly crosslinked polymer networks, J. Polym. Sci. B Polym. Phys. 35 (1997) 2297–2307, https://doi.org/10.1002/(SICI)1099-0488(199710)35:14<2297::AID-POLB10>3.0.CO;2-7.

[3] M.P. Silva, P. Santos, J.M. Parente, S. Valvez, P.N.B. Reis, A.P. Piedade, Effect of post-cure on the static and viscoelastic properties of a polyester resin, Polymers 12 (2020) 1927, https://doi.org/10.3390/polym12091927.

[4] Y.-J. Park, D.-H. Lim, H.-J. Kim, D.-S. Park, I.-K. Sung, UV- and thermal-curing behaviors of dual-curable adhesives based on epoxy acrylate oligomers, Int. J. Adhes. Adhes. 29 (2009) 710–717, https://doi.org/10.1016/j.ijadhadh.2009.02.001.

[5] D.P. Nair, N.B. Cramer, J.C. Gaipa, M.K. McBride, E.M. Matherly, R.R. McLeod, R. Shandas, C.N. Bowman, Two-stage reactivepolymer network forming systems, Adv. Funct. Mater. 22 (2012) 1502–1510, https://doi.org/10.1002/adfm.201102742.

[6] E. Hasa, J.W. Stansbury, C. Allan Guymon, Manipulation of crosslinking in photo-induced phase separated polymers to control morphology and thermo-mechanical properties, Polymer 202 (2020), 122699, https://doi.org/10.1016/j.polymer.2020.122699.

[7] G. González, X. Fernández-Francos, À. Serra, M. Sangermano, X. Ramis, Environmentally-friendly processing of thermosets by two-stage sequential aza-Michael addition and free-radical polymerization ofamine–acrylate mixtures, Polym. Chem. 6 (2015) 6987–6997, https://doi.org/10.1039/C5PY00906E.

[8] A. Retailleau, X. Ibrahim, Allonas, Dual-cure photochemical/thermal polymerization of acrylates: a photoassisted process at low light intensity, Polym. Chem. 5 (2014) 6503–6509, https://doi.org/10.1039/C4PY00548A.

[9] A.L. Kanibolotsky, N.J. Findlay, P.J. Skabara, Polythiophene and oligothiophene systems modified by TTF electroactive units for organic electronics, Beilstein J. Org. Chem. 11 (2015) 1749–1766, https://doi.org/10.3762/bjoc.11.191.

[10] (a) Y. Zhang, C. Ji, Electro-induced covalent cross-linking of chitosan and formation of chitosan hydrogel films: its application as an enzyme immobilization matrix for use in a phenol sensor, Anal. Chem. 12 (2010) 5275–5281, https://doi.org/10.1021/ac100714s;
(b) S. Pöller, D. Koster, W. Schuhmann, Stabilizing redox polymer films by electrochemically induced crosslinking, Electrochem. Commun. 34 (2013) 327–330, https://doi.org/10.1016/j.elecom.2013.07.033.

[11] (a) O. Yurchenko, J. Heinze, S. Ludwigs, Electrochemically induced formation of independent conductivity regimes inpPolymeric tetraphenylbenzidine systems, ChemPhysChem 11 (2010) 1637–1640, https://doi.org/10.1002/cphc.201000131;
(b) P. Reinold, K. Bruchlos, S. Ludwigs, Polym. Chem. 8 (2017) 7351–7359, https://doi.org/10.1039/C7PY01688C.

[12] D. Larumbe, I. Gallardo, C.P. Andrieux, Anodic oxidation of some tertiary amines, J. Electroanal. Chem. 304 (1991) 241–247, https://doi.org/10.1016/0022-0728(91)85506-k.

[13] H. Ishida, Handbook of benzoxazines resins, ed, H. Ishida and T. Agag, Elsevier, Amsterdam, 2011.

[14] N.N. Ghosh, B. Kiskan, Y. Yagci, Polybenzoxazines—New high performance thermosetting resins: Synthesis and properties, Prog. Polym. Sci. 32 (2007) 1344–1391, https://doi.org/10.1016/j.progpolymsci.2007.07.002.

[15] M. Kukut, B. Kiskan, Y. Yagci, Self-curable benzoxazine functional polybutadienes synthesized by click chemistry, Des. Monomers Polym. 12 (2009) 167–176, https://doi.org/10.1163/156855509X412108.

[16] M. Ergin, B. Kiskan, B. Gacal, Y. Yagci, Thermally curable polystyrene via click chemistry, Macromolecules 13 (2007) 4724–4727, https://doi.org/10.1021/ma070549j.
[17] B. Kiskan, G. Demiray, Y. Yagci, Thermally curable polyvinylchloride via click chemistry, J. Polym. Sci. A Polym. Chem. 46 (2008) 3512–3518, https://doi.org/10.1002/pola.22685.
[18] H.-M. Ma, Y. Liu, Y.-X. Liu, J.-J. Qiu, Ch-M. Liu, Vinyl benzoxazine: a novel heterobifunctional monomer can undergo both free radical polymerization and cationic ring-opening polymerization, RSC Adv. 5 (2015) 102441–102447, https://doi.org/10.1039/C5RA18058A.
[19] L. Jin, T. Agag, Y. Yagci, H. Ishida, Methacryloyl-functional benzoxazine: photopolymerization and thermally activated polymerization, Macromolecules 4 (2011) 767–772, https://doi.org/10.1021/ma102351a.
[20] B. Kiskan, Y. Yagci, Self-healing of poly(propylene oxide)-polybenzoxazine thermosets by photoinduced coumarine dimerization, J. Polym. Sci. Part A: Polym. Chem. 52 (2014) 2911–2918, https://doi.org/10.1002/pola.27323.
[21] Ch. Zhou, J. Lin, X. Lu, Z. Xin, Enhanced corrosion resistance of polybenzoxazine coatings by epoxy incorporation, RSC Adv., 6 (2016) 28428–28434, DOI https://doi.org/10.1039/C6RA02215D.
[22] L. Wan, J. Wang, L. Xie, Y. Sun, K. Li, Nitrogen-enriched hierarchically porous carbons prepared from polybenzoxazine for high-performance supercapacitors, ACS Appl. Mater. Interfaces 6 (2014) 15583–15596, https://doi.org/10.1021/am504564q.
[23] B. Gacal, L. Cianga, T. Agag, T. Takeichi, Y. Yagci, Synthesis and characterization of maleimide (co)polymers with pendant benzoxazine groups by photoinduced radical polymerization and their thermal curing, J. Polym. Sci. A Polym. Chem. 45 (2007) 2774–2786, https://doi.org/10.1002/pola.22034.
[24] O. Yurchenko, D. Freytag, L. zur Borg, R. Zentel, J. Heinze, S. Ludwigs, Electrochemically induced reversible and irreversible coupling of triarylamines, J. Phys. Chem. B 116 (2012) 30–39, https://doi.org/10.1021/jp208076z.
[25] L.-C. Lin, H.-J. Yen, Y.-R. Kung, Ch.-M. Leu, T.-M. Lee, G.-S. Liou, Novel near-infrared and multi-colored electrochromic polybenzoxazines with electroactive triarylamine moieties, J. Mater. Chem. C 2 (2014) 7796–7803, https://doi.org/10.1039/C4TC01469C.
[26] D. Shen, C. Liu, R.M. Sebastián, J. Marquet, R. Shönfeld, Understanding the surface properties of polybenzoxazines: Interaction of polybenzoxazine model compounds with metal ions and water, J. Appl. Polym. Sci. 133 (2016) 44099, https://doi.org/10.1002/app.44099.
[27] Y. Sun, N. Zhou, W. Zhang, Y. Li, Z. Cheng, J. Zhu, Z. Zhang, X.J. Zhu, Synthesis of novel side-chain triphenylamine polymers with azobenzene moieties via RAFT polymerization and investigation on their photoelectric properties, Polym. Sci. Part A: Polym. Chem. 50 (2012) 3788, https://doi.org/10.1002/pola.26167.
[28] C. Lee, W. Yang, R.G. Parr, Development of the Colle-Salvetti correlation-energy formula into a functional of the electron density, Phys. Rev. B 37 (1988) 785–789, https://doi.org/10.1103/PhysRevB.37.785.
[29] A.D. Becke, Density-functional thermochemistry. III. The Role of Exact exchange, J. Chem. Phys. 98 (1993) 5648–5652, https://doi.org/10.1063/1.464913.
[30] P.J. Stephens, F.J. Devlin, C.F. Chabalowski, M.J. Frisch, Ab Initio Calculation of Vibrational Absorption and Circular Dichroism Spectra Using Density Functional Force Fields, J. Phys. Chem. 98 (1994) 11623–11627, https://doi.org/10.1021/j100096a001.
[31] S. Grimme, J. Antony, S. Ehrlich, H. Krieg, A Consistent and accurate ab initio parametrization of density functional dispersion correction (DFT-D) for the 94 Elements H-Pu, J. Chem. Phys. 132 (2010), https://doi.org/10.1063/1.3382344.
[32] M.J. Frisch, G.W. Trucks, H.B. Schlegel, G.E. Scuseria, M.A. Robb, J.R. Cheeseman, G. Scalmani, V. Barone, G.A. Petersson, H. Nakatsuji, X. Li, M. Caricato, A.V. Marenich, J. Bloino, B.G. Janesko, R. Gomperts, B. Mennucci, J.B. Hratch, F. Gaussian 16. 2016, p Gaussian, Inc., Wallingford CT, 2016.
[33] A.V. Marenich, C.J. Cramer, D.G. Truhlar, Universal solvation model based on solute electron density and on a continuum model of the solvent defined by the bulk dielectric constant and atomic surface tensions, J. Phys. Chem. B 113 (2009) 6378–6396, https://doi.org/10.1021/jp810292n.
[34] D.A. Case, R.M. Betz, D.S. Cerutti, I.T.E. Cheatham, T.A. Darden, R.E. Duke, T.J. Giese, H. Gohlke, A.W. Goetz, N. Homeyer, S. Izadi, P. Janowski, J. Kaus, A. Kovalenko, T.S. Lee, S. LeGrand, P. Li, C. Lin, T. Luchko, et al. AMBER 2016; University of California: San Francisco, 2016.
[35] J. Wang, R.M. Wolf, J.W. Caldwell, P.A. Kollman, D.A. Case, development and testing of a general amber force field, J. Comput. Chem. 25 (2004) 1157–1174, https://doi.org/10.1002/jcc.20035.
[36] U.C. Singh, P.A. Kollman, An approach to computing clectrostatic charges for molecules, J. Comput. Chem. 5 (1984) 129–145, https://doi.org/10.1002/jcc.540050204.
[37] B.H. Besler, K.M. Merz, P.A. Kollman, Atomic charges derived from semiempirical methods, J. Comput. Chem. 11 (1990) 431–439, https://doi.org/10.1002/jcc.540110404.
[38] T.A. Andrea, W.C. Swope, H.C. Andersen, The role of long ranged forces in determining the structure and properties of liquid aater, J. Chem. Phys. 79 (1983) 4576–4584, https://doi.org/10.1063/1.446373.
[39] H.J.C. Berendsen, J.P.M. Postma, W.F. van Gunsteren, A. DiNola, J.R. Haak, Molecular dynamics with coupling to an external bath, J. Chem. Phys. 81 (1984) 3684–3690, https://doi.org/10.1063/1.448118.
[40] L.A. Kelley, S.P. Gardner, M.J. Sutcliffe, An automated approach for clustering an ensemble of NMR-derived protein structures into conformationally related subfamilies, Protein Eng. Des. Sel. 9 (1996) 1063–1065, https://doi.org/10.1093/protein/9.11.1063.
[41] E.F. Pettersen, T.D. Goddard, C.C. Huang, G.S. Couch, D.M. Greenblatt, E.C. Meng, T.E. Ferrin, UCSF Chimera-A visualization system for exploratory research and analysis, J. Comput. Chem. 25 (2004) 1605–1612, https://doi.org/10.1002/jcc.20084.
[42] X. Ning, H. Ishida, Phenolic materials via ring-opening polymerization: Synthesis and characterization of bisphenol-A based benzoxazines and their polymers, J. Polym. Sci., Part A, Polym. Chem. 32 (1994) 1121–1129, https://doi.org/10.1002/pola.1994.080320614.
[43] B. Kiskan, Adapting benzoxazine chemistry for unconventional Applications, React. Funct. Polym. 129 (2018) 76–88, https://doi.org/10.1016/j.reactfunctpolym.2017.06.009.
[44] I. Hamerton, L.T. McNamara, B.J. Howlin, P.A. Smith, P. Cross, S.J. Ward, Developing toughened aromatic polybenzoxazines using thermoplastic oligomers and telechelics, part 1: Preparation and characterization of the functionalized oligomers, J. Appl. Polym. Sci. 131 (2014), https://doi.org/10.1002/app.40875.
[45] M.C. Celina, N.H. Giron, M.R. Rojo, An overview of high temperature micro-ATR IR spectroscopy to monitor polymer reactions, Polymer 53 (2012) 4461–4471, https://doi.org/10.1016/j.polymer.2012.07.051.
[46] N. Xiang, T. Lee, L. Leung, S. So, J. Shi, M. Gong, Synthesis and photoluminescence of two novel bipolar organic compounds, Acta Chim. Sinica 64 (2006) 1157–1162 (In chinese).
[47] H. Stutz, K.-H. Illers, J. Mertesa, Generalized theory for the glass transition temperature of crosslinked and uncrosslinked polymers, J. Polym. Sci.: Part B: Polym. Phys. 28 (1990) 1483–1498, https://doi.org/10.1002/polb.1990.090280906.
[48] G.R. Goward, D. Sebastiani, I. Schnell, H.W. Spiess, H.-D. Kim, H. Ishida, Benzoxazine Oligomers: Evidence for a Helical Structure from Solid-State NMR Spectroscopy and DFT-Based Dynamics and Chemical Shift Calculations, J. Am. Chem. Soc. 125 (19) (2003) 5792–5800, https://doi.org/10.1021/ja029059r.
[49] H.Ch Moon, C.-H. Kim, T.P. Lodge, C.D. Frisbie, Multicolored, Low-power, flexible electrochromic devices based on ion gels, ACS Appl. Mater. Interfaces 8 (2016) 6252–6260, https://doi.org/10.1021/acsami.6b01307.
[50] M. Villabona, M. Benet, S. Mena, R.-O. Al-Kaysi, J. Hernando, G. Guirado, Multistimuli-responsive fluorescent switches based on spirocyclic meisenheimer compounds: smart molecules for the design of optical probes and electrochromic materials, J. Org. Chem. 83 (2018) 9166–9177, https://doi.org/10.1021/acs.joc.8b01211.
[51] S. Santiago, M. Aller, F.J. del Campo, G. Guirado, Screen-printable electrochromic polymer inks and ion gel electrolytes for the design of low-power, flexible electrochromic devices, Electroanalysis 31 (2019) 1664–1671, https://doi.org/10.1002/elan.201900154.